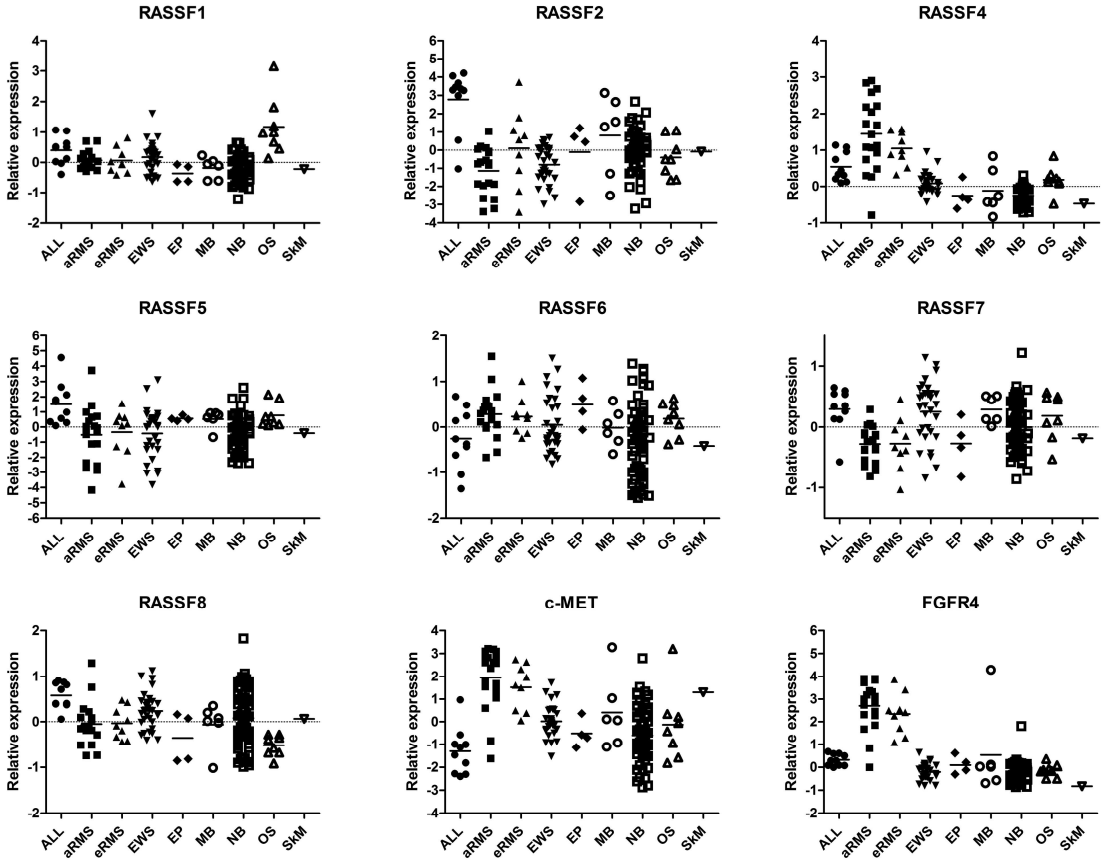

Supplemental Figure 1. RASSF expression profile in pediatric tumor cell lines and xenografts. Median-centered Log_2 values of pediatric cancer cell lines and xenografts, as obtained from http://home.ccr.cancer.gov/oncology/oncogenomics/. ALL, acute lymphoblastic leukemia, aRMS, alveolar rhabdomyosarcoma, eRMS, embryonal rhabdomyosarcoma, EWS, Ewing's sarcoma, EP, ependymoma, MB, meduloblastoma, NB, neuroblastoma, OS, osteosarcoma, SkM, normal skeletal muscle. No data was available for RASSFs 3, 9, and 10.

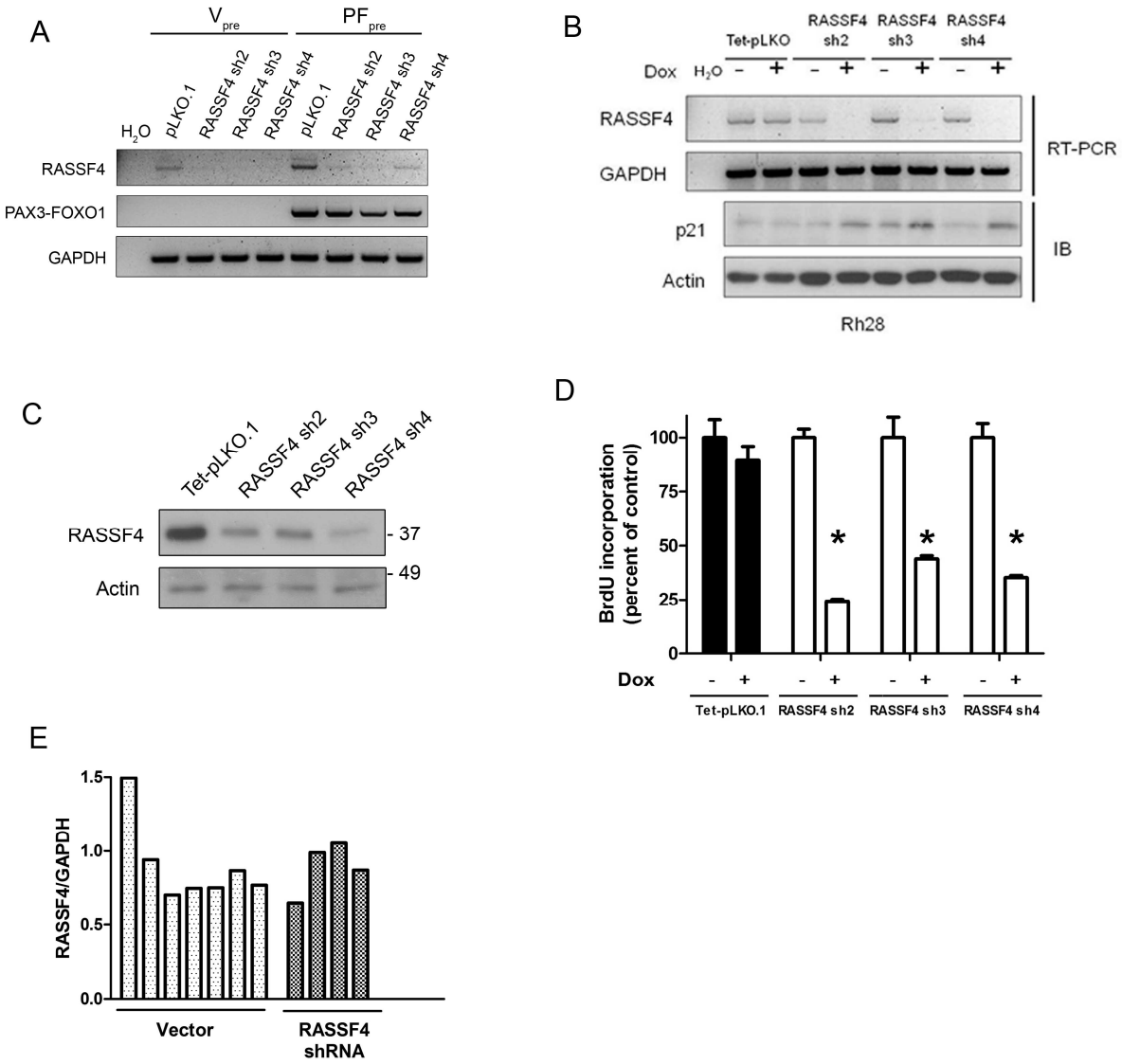

Supplemental Figure 2. RASSF4 shRNA validation (A) Constititive RASSF4 shRNA validation in primary HSMM cells expressing vector (Vpre) or PAX3-FOXO1 (PFpre), as measured by semi-quantitative PCR. Validation of docycline-inducible RASSF4 shRNA *in vitro* in Rh28 cells by semi-quantitative RT-PCR, p21 immunoblot (**B**), endogenous RASSF4 levels in doxycycline-treated cells (**C**), and BrdU incorporation assay (**D**). (**E**) Rh28 xenografts in the absence of doxycycline have no effect on RASSF4 expression levels.

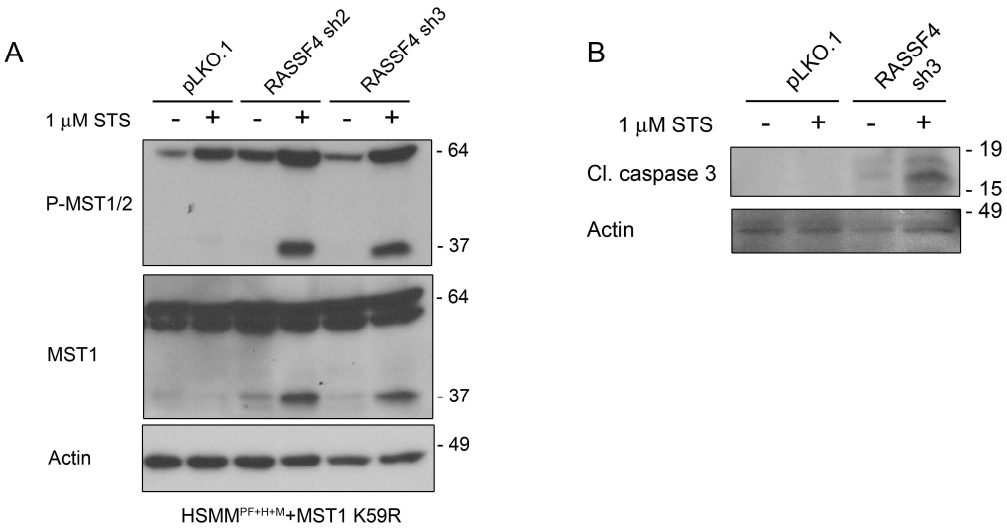

Supplemental Figure 3. RASSF4-deficient cells display increased STS-induced MST1 and caspase 3 cleavage. (A) RASSF4 deficiency causes MST1 phosphorylation and cleavage upon staurosporine (STS) treatment. Cells expressing FLAG-MST1 K59R were treated for 1 hour with 1uM STS and examined for phospho-MST1/2 and total MST1 by immunoblot. (**B**) Upon 1hr treatment with 1μM STS, RASSF4-deficient aRMS cells display higher cleaved caspase 3 as measured by immunoblot. In A-B, actin is used as a loading control.

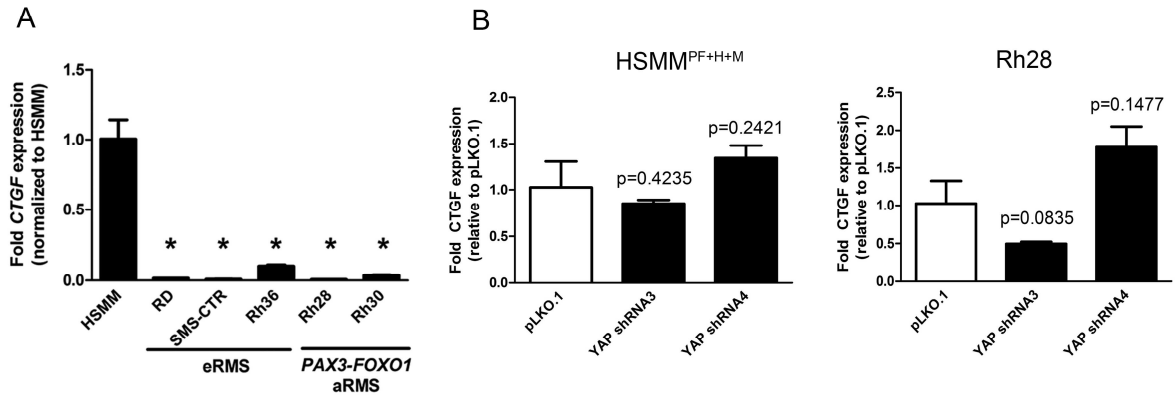

Supplemental Figure 4. CTGF levels in aRMS cells and YAP knockdown cells. (A) CTGF levels in RMS cells as measured by real-time PCR. (**B**) CTGF levels are unchanged in YAP-deficient aRMS cells.

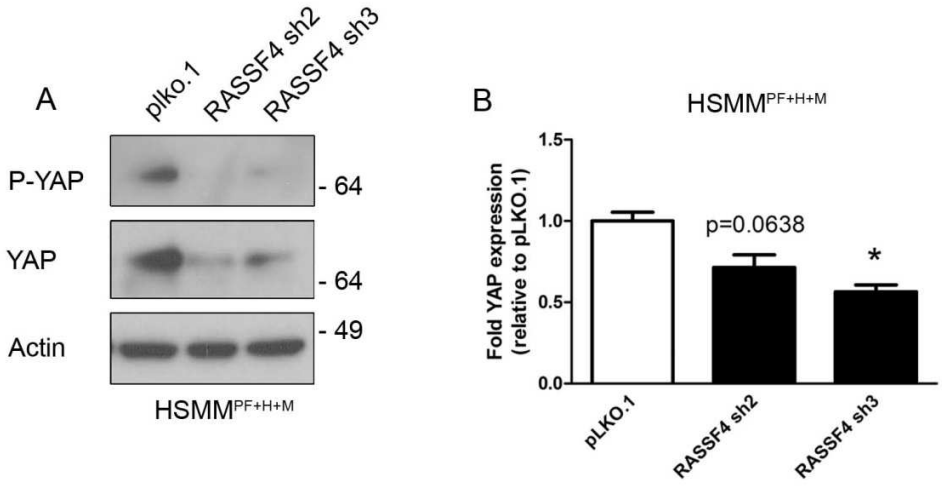

Supplemental Figure 5. Effects on YAP protein and mRNA levels in RASSF4-knockdown cells. (A) RASSF4-deficient HSMM^{PF+H+M} cells display lower levels of P-YAP (S127) and YAP protein as measured by immunoblot. (**B**) Changes in YAP mRNA levels in RASSF4-deficient aRMS cells.

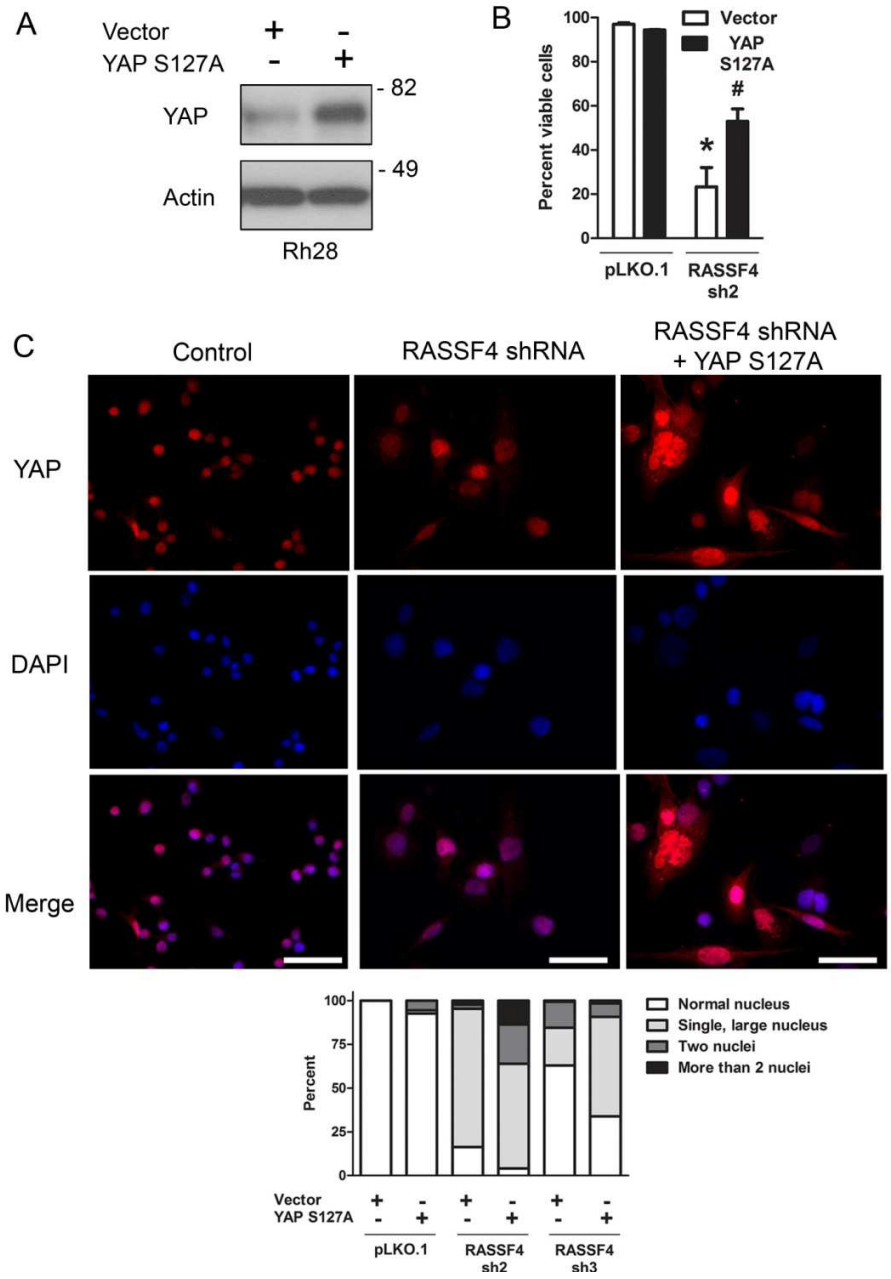

Supplemental Figure 6. Effects of YAPS127A expression on RASSF4 loss. (**A**) Immunoblot validation of YAP S127A-expressing Rh28 aRMS cell lines. (**B**) Rh28 cells expressing YAP S127A maintain better cell viability with RASSF4 knockdown compared to cells with RASSF4 knockdown alone. Error bars represent SD. *p=0.004 comparing vector cells, pLKO.1 to RASSF4 sh2. #p=0.016 comparing RASSF4 shRNA cells vector to YAP S127A. (**C**) RASSF4 knockdown cells display mitotic defects, which are more prevalent with YAPS127A expression. Scalebar = 50µm.

Supplemental Table 1

Oligos used to generate shRNAs	
Oligo	**Sequence (5'-3')**
RASSF4 shRNA2 FW	CCGGCATCAGTGACAGCAAGTCCATCTCGAGATGGACTTGCTGTCACTGATGTTTTTG
RASSF4 shRNA2 REV	AATTCAAAAACATCAGTGACAGCAAGTCCATCTCGAGATGGACTTGCTGTCACTGATG
RASSF4 shRNA3 FW	CCGGGTACCCGCTGATTTCCAGAATCTCGAGATTCTGGAAATCAGCGGGTACTTTTTG
RASSF4 shRNA3 REV	AATTCAAAAAGTACCCGCTGATTTCCAGAATCTCGAGATTCTGGAAATCAGCGGGTAC
RASSF4 shRNA4 FW	CCGGGCTGCAAGAAACACGGTCATTCTCGAGAATGACCGTGTTTCTTGCAGCTTTTTG
RASSF4 shRNA4 REV	AATTCAAAAAGCTGCAAGAAACACGGTCATTCTCGAGAATGACCGTGTTTCTTGCAGC
YAP shRNA 3 FW	CCGGCCCAGTTAAATGTTCACCAATCTCGAGATTGGTGAACATTTAACTGGGTTTTTG
YAP shRNA3 REV	AATTCAAAAACCCAGTTAAATGTTCACCAATCTCGAGATTGGTGAACATTTAACTGGG
YAP shRNA4 FW	CCGGGCCACCAAGCTAGATAAAGAACTCGAGTTCTTTATCTAGCTTGGTGGCTTTTTG
YAP shRNA4 REV	AATTCAAAAAGCCACCAAGCTAGATAAAGAACTCGAGTTCTTTATCTAGCTTGGTGGC
Oligos used to clone HA-RASSF4	
Oligo	**Sequence (5'-3')**
HA-RASSF4 FW	TAATCCCCCGGGCCACCATGTACCCATACGACGTCCCAGACTACGCTATGAAGGAAGACTGTCTGCCG
RASSF4 REV	TCTCACTTCTTCAGTTCAATACAGC
RASSF4ΔSARAH REV	TAATCCGTCGACTCAGACTTCATGGGGGACTTCC
Oligos used for semi-quantitative RT-PCR	
Oligo	**Sequence (5'-3')**
RASSF4 FW	GAAGACTGTCTGCCGAGTTC
RASSF4 REV	CTGTCTGTGGAACTCTCAGC
HDAC9 FW	TCCACATGAACAAACTGCTTTCGAAA
HDAC9 REV	TCCATTTACCAAACCTGCAATGCAT
DUSP4 FW	TTAGCTCTCGCCCGCCCCTTT
DUSP4 REV	TCCTTCACGGCATCGATGTACTCT
SPRY4 FW	GCCTTGCCGGTTCCTCCGAC
SPRY4 REV	AGGCTTCTAGGGGCCTTTGAGGA
CXCR4 FW	GTGGGCGGGGCAGAGGAGTTA
CXCR4 REV	GGAGGTCGGCCACTGACAGGT
FGFR4 FW	AAACCAGCAACGGCCGCCTG
FGFR4 REV	GTCGAGGTACTCCTCAGAGAC
MYOD FW	TAGGGTCCCTCGCGCCCAAA
MYOD REV	GCGGCCATCGCAATGGGTCT
MEF2A FW	AGAGGGTGCGACAGCCCAGAC
MEF2A REV	TGCCCTCCAGCAACAAGAGAGC
PAX3-FOXO1 FW	CCCACTGCCATGCCGACCTTG
PAX3-FOXO1 REV	ACGAATTGAATTCTGAGGTGAGAG
GAPDH FW	GAGAGACCCTCACTGCTG
GAPDH REV	GATGGTACATGACAAGGTGC
Oligos used for qPCR	
Oligo	**Sequence (5'-3')**
RASSF4 FW	TTC TCT ATC AAC GGC CAC TTC
RASSF4 REV	CTT CCA CCC TAA ATT TGT TCA GC
YAP1 FW	CCT TCT TCA AGC CGC CGG AG
YAP1 REV	CAG TGT CCC AGG AGA AAC AGC
CTGF FW	GCA GAG CCG CCT GTG CAT GG
CTGF REV	GGT ATG TCT TCA TGC TGG
GAPDH FW	ATG GGG AAG GTG AAG GTC G
GAPDH REV	GGG GTC ATT GAT GGC AAC AAT A

Supplemental Experimental Procedures

Generation of Cell Lines and Plasmids. Human skeletal muscle myoblasts (HSMMs) stably expressing *PAX3-FOXO1, hTERT*, and *MycN* have been described previously (Naini et al., 2008), and were maintained in defined media (SkGM-2 Bullet Kit, Lonza). Human RMS cell lines (RD, SMS-CTR, Rh3,

Rh28, Rh30, and Rh36) were a gift from Dr. Tim Triche of Children's Hospital of Los Angeles, grown in RPMI-1640 (GIBCO) with 10% FBS, and authenticated by PCR-based documentation of *PAX3-FOXO1* (for aRMS) within six months of use in experiments. It is of note that the Rh3 and Rh28 cell lines have been shown to be derived from the same patient (Barr et al., 1998). RASSF4 shRNA plasmids were generated using annealed oligonucleotides (*table below*) and ligated into the EcoRI/AgeI sites of pLKO.1 or Tet-pLKO-puro (obtained from Addgene, plasmids #10878 and 21915). The human RASSF4 I.M.A.G.E. clone (5527647) was obtained from ATCC and confirmed by diagnostic digest and sequencing. HA-RASSF4 and HA-RASSF4ΔSARAH were generated by PCR amplification using primers described in Supplemental Table I. PCR products were digested with SmaI and SalI and cloned into either pBabePuro (BamHI-Klenow/SalI) or pRRLSIN.cPPT.PGK-GFP.WPRE (BamHI-Klenow/SalI, Addgene plasmid #12252). pCMV5-MST1 and pCMV5-MST1K59R expression plasmids were purchased from Addgene (plasmid #1965, 1966). MST1 plasmids were sublconed into pRRLSIN.cPPT.PGK-GFP.WPRE by digesting MST1 plasmids with BamHI/NotI-Kleenow and pRRLSIN.cPPT.PGK-GFP.WPRE with BamHI/SalI-Kleenow. Plasmids were verified by restriction digest and DNA sequencing. Lentiviral particles were produced from HEK293T cells transiently transfected with the lentiviral expression plasmid, pMDM2.G (Addgene plasmid #12259) and psPAX2 (Addgene plasmid #12260) as described in the RNAi Consortium protocol (http://www.broadinstitute.org/rnai/public/resources /protocols). Lentiviral particles were harvested 48 hours post-transfection and passed through a 0.45 μM filter. Polybrene was added to a final concentration of 4 μg/mL prior to lentiviral transduction of aRMS cell lines.

Immunoprecipitation (IP) and Immunoblotting. Cells were lysed in Tris/RIPA or 20mM Tris pH7.5, 1% NP-40, 137mM NaCl, 10% glycerol, 0.1mM EDTA, 0.1mM EGTA (for IPs) supplemented with protease and phosphatase inhibitors. Protein concentration was measured by DC assay (Bio-Rad). IPs for hemagglutinin (HA) – tagged proteins were performed with anti-HA (12CA5, Roche) and protein G Agarose (Santa Cruz). Lysate or IP'ed protein was resolved by SDS-PAGE, transferred to PVDF membrane

and immunoblotted with primary and secondary antibodies: phospho-MST1/2 (Thr183/Thr180), MST1, phospho-YAP (Ser 127), YAP, phospho-LATS1 (Ser909), LATS1, phospho-Mob1 (Thr35), Mob1 (Cell Signaling), HA (Roche), Erk1 (Santa Cruz), RASSF4, anti-actin (Sigma), RASSF4 (Novus Biologicals), Pan-Ras (detects H-, K-, and N-Ras, Calbiochem), HRP-labeled goat anti-mouse or anti-rabbit antibody (Invitrogen-Zymed).

Immunohistochemistry and Immunofluorescence Tumor xenografts were fixed overnight in 4% paraformaldehyde (Sigma) and paraffin embedded. Xenografts were sectioned and stained with H&E to assess tumor morphology, and Ki67 (Thermo Scientific) to assess tumor cell proliferation as previously described (Crose et al., 2012). Images were obtained on an Olympus Vanox AH-3 Microscope using an Olympus DP70 Digital Microscope Camera. For immunofluorescence experiments, cells grown on coverslips were fixed in 4% paraformaldehyde for 14 minutes, followed by 3 washes with PBS. Coverslips were blocked in 5% goat serum/0.3% Triton X-100 in PBS, followed by incubation in primary antibody, diluted in 1% BSA/0.3%Triton X-100 in PBS, overnight at 4^{o}. Coverslips were washed 5 times over the course of 45 minutes, followed by incubation in flourochrome-conjugated secondary antibody, diluted in 1% BSA/0.3%Triton X-100 in PBS for 1 hour at room temperature. Coverslips were treated with 300 nM DAPI in PBS followed by 45 minutes of PBS washes. Coverslips were mounted on slides using Fluoromount-G (SouthernBiotech). Images were collected on a Nikon Eclipse TE2000-U microscope with a CoolSnap HQ camera using NIS elements software. Images were pseudocolored and merged using ImageJ.

Cell Viability Assay. Cell viability was assayed using standard Trypan blue staining followed by manual cell counts on a hemocytometer.

***Drosophila* Genetics and Expression Profiling.** In a screen for PAX7-FOXO1 suppressors, the UAS-PAX7-FOXO1 and Myosin Heavy Chain-Gal4 transgenes were used, and lethality assessed, as previously

described (Avirneni-Vadlamudi et al., 2012; Galindo et al., 2006). In this system, F_1 progeny males express PAX7-FOXO1, while female siblings do not. The *Df(3L)Exel*^{6087}, *Df(3L)vin5*, *Df(3L)GN24*, *Df(3L)Exel*^{6193}, *dRASSF*^{DG30608}, *dRASSF*^{A531}, and *Df(2R)BSC22* stocks were obtained from the Bloomington *Drosophila* Stock Center. Microarray analysis was performed as described previously, with raw data available in the ArrayExpress database (accession number E-MTAB-839).

References

Avirneni-Vadlamudi, U., Galindo, K.A., Endicott, T.R., Paulson, V., Cameron, S., and Galindo, R.L. (2012). Drosophila and mammalian models uncover a role for the myoblast fusion gene TANC1 in rhabdomyosarcoma. J Clin Invest *122*, 403-407.

Barr, F.G., Nauta, L.E., and Hollows, J.C. (1998). Structural analysis of PAX3 genomic rearrangements in alveolar rhabdomyosarcoma. Cancer Genet Cytogenet *102*, 32-39.

Crose, L.E., Etheridge, K.T., Chen, C., Belyea, B.C., Jones, L.T., Bentley, R.C., and Linardic, C.M. (2012). FGFR4 blockade exerts distinct anti-tumorigenic effects in embryonal versus alveolar rhabdomyosarcoma. Clin Cancer Res.

Galindo, R.L., Allport, J.A., and Olson, E.N. (2006). A Drosophila model of the rhabdomyosarcoma initiator PAX7-FKHR. Proc Natl Acad Sci U S A *103*, 13439-13444.

Naini, S., Etheridge, K.T., Adam, S.J., Qualman, S.J., Bentley, R.C., Counter, C.M., and Linardic, C.M. (2008). Defining the cooperative genetic changes that temporally drive alveolar rhabdomyosarcoma. Cancer Res *68*, 9583-9588.